Stability and Structure of Oligomers of the Alzheimer Peptide Aβ_{16-22}: From the Dimer to the 32-Mer

Ute F. Röhrig,* Alessandro Laio,[†] Nazario Tantalo,*[‡] Michele Parrinello,[†] and Roberto Petronzio[‡§]

*Centro Studi e Ricerche "Enrico Fermi", Compendio Viminale, Rome, Italy; [†]Computational Science, Department of Chemistry and Applied Biosciences, ETH Zurich, Lugano, Switzerland; [‡]Istituto Nazionale di Fisica Nucleare, Sezione di Roma Tor Vergata, Rome, Italy; and [§]Physics Department, University of Rome Tor Vergata, Rome, Italy

ABSTRACT   Several neurodegenerative diseases such as Alzheimer's, Parkinson's, and Huntington's diseases are associated with amyloid fibrils formed by different polypeptides. We probe the structure and stability of oligomers of different sizes of the fragment Aβ_{16-22} of the Alzheimer β-amyloid peptide using atomic-detail molecular dynamics simulations with explicit solvent. We find that only large oligomers form a stable β-sheet aggregate, the minimum nucleus size being of the order of 8–16 peptides. This effect is attributed to better hydrophobic contacts and a better shielding of backbone-backbone hydrogen bonds from the solvent in bigger assemblies. Moreover, the observed stability of β-sheet aggregates with a different number of layers can be explained on the basis of their solvent-accessible surface area. Depending on the stacking interface between the sheets, we observe straight or twisted structures, which could be linked to the experimentally observed polymorphism of amyloid fibrils. To compare our 32-mer structure to experimental data, we calculate its x-ray diffraction pattern. Good agreement is found between experimentally and theoretically determined reflections, suggesting that our model indeed closely resembles the structures found in vitro.

INTRODUCTION

Several neurodegenerative diseases such as Alzheimer's, Parkinson's, and Huntington's diseases are associated with amyloid fibrils formed by various polypeptides (1–3). In Alzheimer's disease, the insoluble fibrils formed by Aβ_{1-40} and Aβ_{1-42} have long been thought to be neurotoxic (4). However, increasing evidence suggests a strong correlation between dementia and soluble oligomers of these peptides (5–8). Recent experimental data points to the involvement of 12-mers in memory loss (9,10). Therefore the understanding of the structure and dynamics of aggregates of a few peptides is of great biomedical interest. In addition to their biomedical relevance, amyloid fibrils are self-assembling nanostructures, and some novel materials have been developed based on these (11,12).

Due to their noncrystalline and insoluble nature, experimental determination of the atomic structure of amyloid fibrils poses severe challenges. Structural information comes primarily from x-ray and electron diffraction measurements, solid-state NMR spectroscopy, and transmission electron microscopy. The fibrils are typically 50–150 Å in diameter and >1-μm in length, often with a periodic twist. X-ray diffraction yields the characteristic "cross-β" pattern, which is one of the defining features of amyloid fibrils (13–15). This pattern is generally interpreted as indicating the presence of ribbonlike β-sheet structures, with peptide chains in β-strand conformation running roughly perpendicular to the long axis of the fibrils and hydrogen bonds between peptides running roughly parallel to the long axis. The observed periodicities are attributed to the spacing between peptide chains within a

sheet (4.8 Å) and spacing between β-sheet layers (8–13 Å). The similarity of the diffraction patterns of fibrils formed from different peptides and proteins point to a similarity of the underlying physical principles. Recently, the atomic structure of the cross-β spine of some amyloid-forming peptides has been determined in greater detail by electron and x-ray diffraction of microcrystals (16,17). Another set of recent experiments has shown that the peptide sequence does not uniquely determine the structure of the amyloid fibril. A single peptide can exhibit different morphologies (e.g., twisted or untwisted) and different toxicities (18–21). Different morphologies can be obtained by subtle pH or temperature variations, and they are self-propagating when fibrils grow from preformed seeds.

Information about the mechanism of amyloid fibril formation may open the way to novel therapeutic approaches as well as to the development of new nanomaterials. In general, the first step of amyloid fibril formation is considered to be a nucleation process in which proteins or peptides slowly associate to form a nucleus, followed by a much faster propagation reaction, where the nucleus grows by the sequential incorporation of molecules (22–25). However, depending on experimental conditions, non-nucleation-dependent pathways have also been found (19,26). Once amyloid fibrils are formed, they rearrange by dissociation and reassociation of peptides or by reptation of polypeptide strands within an aggregate (27–29). It has been shown that charge attraction and β-propensity favor amyloid fibril formation (30).

In view of the difficulty of determining amyloid fibril structures and aggregation mechanisms through experiment, computer simulations are a natural tool to approach this problem (31–45). In this work we focus on the peptide Aβ_{16-22} (KLVFFAE), which constitutes the central hydrophobic core

of the physiologically relevant Alzheimer peptides $A\beta_{1-40}$ and $A\beta_{1-42}$. $A\beta_{16-22}$ has been shown experimentally to form amyloid fibrils made of in-register antiparallel β sheets (46). Previous molecular dynamics (MD) studies of $A\beta_{16-22}$ have established that in agreement with experiment, an antiparallel alignment of the peptides is most stable (32). In addition, a parallel stacking of β-sheets is suggested. However, the intersheet distance found in these simulations (12 Å) is larger than the experimentally observed distance of 9.9 Å (46). In other computer simulations, the $A\beta_{16-22}$ monomer has been shown to exist predominantly in random coil conformation (33,47). The aggregation mechanism of $A\beta_{16-22}$ oligomers (dimers through hexamers) has been investigated in different works (33,47–49) and a preference for an antiparallel β-sheet alignment has been found.

Here, we systematically study different arrangements of $A\beta_{16-22}$ oligomers (2–4, 8, 16, and 32 peptides) and test their structure and stability in long all-atom explicit-solvent MD simulations.

Anticipating the results from our MD simulations, we find that only the large β-sheet aggregates are stable on the simulation timescale (20–100 ns). While a β-sheet dimer breaks up after a few tens of nanoseconds, the trimer and tetramer take a significantly longer time, and higher oligomers do not break up during the course of the simulations. Assemblies of eight peptides are generally stable but show a rotation of one sheet with respect to the other. The biggest tested assemblies of two and four β-sheets consisting of eight peptides each show very high structural stability, indicating that this could

be the size of the critical nucleus. Since a lateral assembly of four-to-six sheets has been postulated to be involved in the formation of protofilaments (50,51), our largest oligomer approaches experimental stacking sizes.

We find that the relative stability of single-layered and double-layered β-sheet structures of the same number of peptides is directly related to their solvent-accessible surface area (SASA). While in case of four peptides the single-layered and the double-layered structures show similar stabilities and similar surface areas, in case of the octamer a double-layered structure is clearly more stable in the simulations and shows at the same time a significantly smaller surface area.

We also investigate the structural properties of aggregates formed by 16 $A\beta_{16-22}$ peptides. There are six distinct possibilities to stack two in-register antiparallel sheets of $A\beta_{16-22}$ onto each other (Fig. 1), since the three possible interfaces (formed by interaction of the amino-acid side-chains KVFE-LFA, KVFE-KVFE, or LFA-LFA) can be stacked in a parallel or in an antiparallel fashion. Here, we investigate a number of β-sheet stackings that have not been simulated before. Depending on the interface, we observe flat or twisted structures. This is an indication that the different stacking may lead to the different fibril morphologies found in vitro. This result is consistent with recent findings for the case of $A\beta_{1-42}$, where different morphologies are attributed to different interfaces between sheets (52).

Finally, we compare our largest structure with available experimental data by calculating the x-ray diffraction pattern of this system. Even if our sample is much shorter than
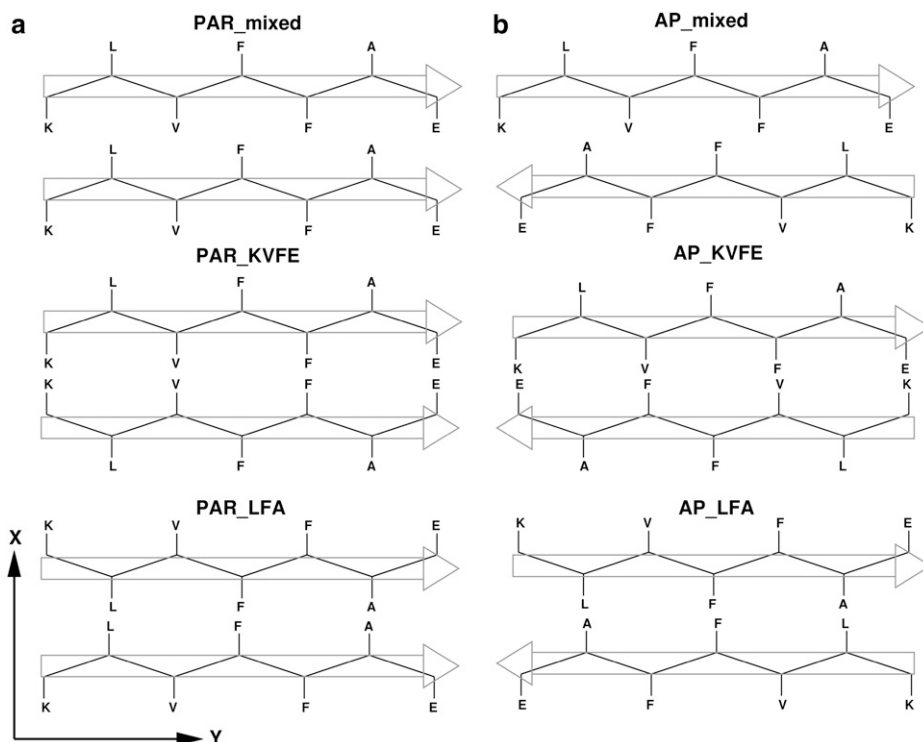

FIGURE 1 Possible stacking of two β-sheets of $A\beta_{16-22}$. (*a*) Parallel stacking; (*b*) antiparallel stacking. The fibril axis (*z* axis) is perpendicular to the paper plane. To generate antiparallel β-sheets, the next layer in z-direction is obtained from the represented one by a rotation of 180° around the *x* axis.

experimental fibrils, we obtain peaks with signaling periodicities that are in good agreement with experimental results.

METHODS

Structures and nomenclature

The peptide Aβ_{16-22} (KLVFFAE) is terminated by an acetyl-group at the N-terminus and by an N-methyl group at the C-terminus. The Lys residue bears a positive charge and the Glu residue a negative charge, so that the total charge of the peptide is zero.

All MD simulations have been carried out starting from an antiparallel β-sheet structure of the Aβ_{16-22} peptides.

As mentioned in the Introduction and represented in Fig. 1, there are three possible distinct interfaces when stacking two β sheets on to each other. The interface can be formed by interactions of the side-chains KVFE-LFA (''mixed''), KVFE-KVFE (''KVFE''), or LFA-LFA (''LFA''). Since all three interfaces can be stacked either in a parallel (**PAR**) or in an antiparallel (**AP**) fashion, corresponding to a shift of one peptide in z-direction in an infinitely long β-sheet, a total of six stacking possibilities of two antiparallel β-sheets exist. In most simulations, we chose conformation **PAR$_{mixed}$** as a starting structure. For a parallel stacking (suggested as being the most stable in earlier MD studies (32)), this seems to provide the best hydrophobic contacts without bringing like charges into close proximity. In 16-Mer (see Results and Discussion, below), we will assess the influence of different stackings (**PAR$_{mixed}$**, **PAR$_{KVFE}$**, **PAR$_{LFA}$**, and **AP$_{LFA}$**) upon the structure of the 16-mer.

Molecular dynamics simulations

The all-atom AMBER/parm99 force field (53) is used for the peptide, whereas water is modeled by the TIP3P force field (54). MD simulations are carried out with the GROMACS code (55–57), using periodic boundary conditions and a cubic simulation cell. Electrostatic interactions are calculated with the Ewald particle-mesh method (58) with a grid spacing of 1.2 Å and a spline interpolation of order 4. We use a cutoff of 10 Å for the real-space direct sum part of the Ewald sum and for the van der Waals interactions. The time integration step is set to 2 fs for simulations at 300 K and to 1 fs for simulations at higher temperature. Simulations at 348 K (75°C) have been carried out for some systems. This temperature has been used to accelerate amyloid fibril formation and reorganization experimentally (29). Rigid bonds involving hydrogen atoms are constrained using the LINCS algorithm (59). The system is coupled to a barostat (60) with a relaxation time of 1 ps. The solute and the solvent are separately coupled to two thermostats (60), which have a relaxation time of 0.2 ps. The initial structures are equilibrated for at least 1 ns using distance restraints on the backbone hydrogen bonds and dihedral restraints on the ϕ- and ψ-angles of the central five amino acids.

While experimental concentrations are usually in the micromolar range, we are restricted to millimolar concentrations (20–150 mmol/l) due to the finite system size. We chose a sodium and chloride ion concentration close to the physiological value (150 mmol/l) for all systems with more than eight peptides, while the smaller oligomers were simulated in pure water. The length of one fully extended peptide is 28 Å. Therefore, to prevent direct interaction between periodic images, the edge length of the cell has to be at least this length plus the cutoff distance ($\approx$40 Å).

The shortcoming of using a small simulation box is evident in a preliminary simulation of a 16-mer, which used a box of the dimensions 70 × 50 × 45 Å^3. In this simulation the solute spontaneously rotated, leading to an artificial direct interaction between periodic images. Therefore large cubic cells were used in the production runs. For other details of the simulations see Table 1.

Analysis

In all figures and in the following discussion, the coordinates are defined as follows: the x axis points in the sheet-stacking direction, the y axis points in the

TABLE 1   Summary of the molecular dynamics simulations

Simulation	N_{Pep}	T [K]	N_{Atoms}	d [Å]	t [ns]
2$_{300}$	2	300	7417	42	90
3$_{300}$	3	300	10962	48	80
4$_{300}$	4	300	13049	51	50
4$_{348}$	4	348	13049	52	70
4$_{300}$/PAR$_{mixed}$	4	300	13049	51	20
4$_{348}$/PAR$_{mixed}$	4	348	13049	52	100
4$_{300}$/AP$_{mixed}$	4	300	13049	51	70
8$_{348}$	8	348	21406	61	24
8$_{300}$/PAR$_{mixed}$	8	300	21406	60	60
8$_{348}$/PAR$_{mixed}$	8	348	21406	61	30
16$_{300}$/PAR$_{mixed}$	16	300	36202	72	40
16$_{348}$/PAR$_{mixed}$	16	348	36202	73	20
16$_{300}$/PAR$_{KVFE}$	16	300	36202	72	50
16$_{300}$/PAR$_{LFA}$	16	300	36202	72	30
16$_{300}$/AP$_{LFA}$	16	300	36202	72	30
32$_{300}$/PAR$_{mixed}$	32	300	34195	70	40
32$_{348}$/PAR$_{mixed}$	32	348	34195	71	30

N_{Pep} is the number of peptides, T the temperature, N_{Atoms} the total number of atoms, d the edge length of the cubic simulation cell, and t the total simulated time. Nomenclature for stacking described in Structures and Nomenclature.

peptide-backbone direction, and the z axis points in the backbone hydrogen-bonding direction (fibril axis).

A hydrogen bond is assumed to be present if the distance between hydrogen donor and acceptor is ≤3.5 Å, and the angle between donor-hydrogen-acceptor deviates by at most 30° from 180°. Secondary structure content is calculated according to the DSSP criteria, (61) using the program with the same name. All reported root mean-square deviations (RMSDs) were calculated with respect to the backbone heavy atoms.

Polar and hydrophobic coordination numbers (CN) between two groups of atoms belonging to different peptides or β-sheets are calculated as

$$CN = \sum_{\substack{i \in Group1 \\ j \in Group2}} \frac{1 - (r_{ij}/r_0)^{10}}{1 - (r_{ij}/r_0)^{20}}. \quad (1)$$

For polar CNs, all hydrogen donors and acceptors are considered (19 atoms per peptide) and a cutoff distance r_0 of 3.5 Å is used, as in the case of hydrogen bonds. For hydrophobic CNs, all side-chain carbon atoms with an absolute charge of <0.4 are considered (30 per peptide) and a cutoff of 4.0 Å is chosen to describe van der Waals contacts.

The solvent-accessible surface area (SASA) is calculated using the program SurfRace (62). Only heavy atoms of the solute are considered. All oxygen and nitrogen atoms are classified as hydrophilic whereas all carbon atoms are classified as hydrophobic. The radius of the solvent probe is 1.4 Å. The van der Waals radii are taken from Richards (63).

Calculation of the x-ray diffraction pattern

In a noncrystalline structure, it is not possible to define in a unique manner the distance between two adjacent peptides within a sheet (d_P) or the distance between two adjacent sheets (d_S). For example, one could approximate d_P by taking pairs of atoms (one per peptide) and measuring the minimal distance within this set, or alternatively one could fit two parallel lines to the two peptide backbones and measure their distance. To avoid these ambiguities and to extract quantities from our MD simulations that can be directly compared with available experimental data, we have calculated the trajectory average of the x-ray diffraction pattern of our largest simulated system (**32$_{300}$/PAR$_{mixed}$**).

The scattering is calculated from the heavy atoms of the solute only, and the fibril axis is aligned with the z axis. The x-ray scattering amplitude is a function of the scattering vector $\vec{q}$ and is defined as

$$A(\vec{q}) = \sum_i b_i(q) e^{-i\vec{q}\cdot\vec{r}_i}, \qquad (2)$$

where the index i runs over all atoms and the atomic form factors b_i are taken from Chantler (64) and Richards (65). The scattering intensity I is obtained by averaging the square modulus of the amplitude over the MD trajectory,

$$I(\vec{q}) = \sum_{i,j} b_i(q) b_j(q) \langle e^{-i\vec{q}\cdot(\vec{r}_i - \vec{r}_j)} \rangle_{MD}. \qquad (3)$$

We consider an incident x-ray beam parallel to the y axis of fixed wavelength λ, and we calculate the scattering intensity as a function of the outgoing direction (θ, ϕ):

$$\vec{q} = \vec{k}_i - \vec{k}_o, \quad \vec{k}_i = \frac{2\pi}{\lambda}(0, 1, 0),$$

$$\vec{k}_0 = \frac{2\pi}{\lambda}(\cos\phi\cos\theta, \cos\phi\sin\theta, \sin\phi). \qquad (4)$$

RESULTS AND DISCUSSION

Dimer

An antiparallel in-register β-sheet consisting of two peptides was used as an initial guess for the dimer structure (Fig. 2 a). The dimer is not stable as constructed, but disruption is slow on the simulation timescale, indicating that a very long simulation time is compulsory for assessing the stability of the system. A sequence of snapshots in Fig. 2 a illustrates how the disruption process proceeds. After 5 ns the β-content is significantly reduced from its initial value of 10 residues (Fig. 2 b). At 20 ns, no appreciable β-content can be measured anymore, but a significant amount of hydrophobic and polar contacts still remains. The polar contacts are lost after ~30 ns. Only later (45 ns) the hydrophobic interactions also become negligible and the two peptides become completely
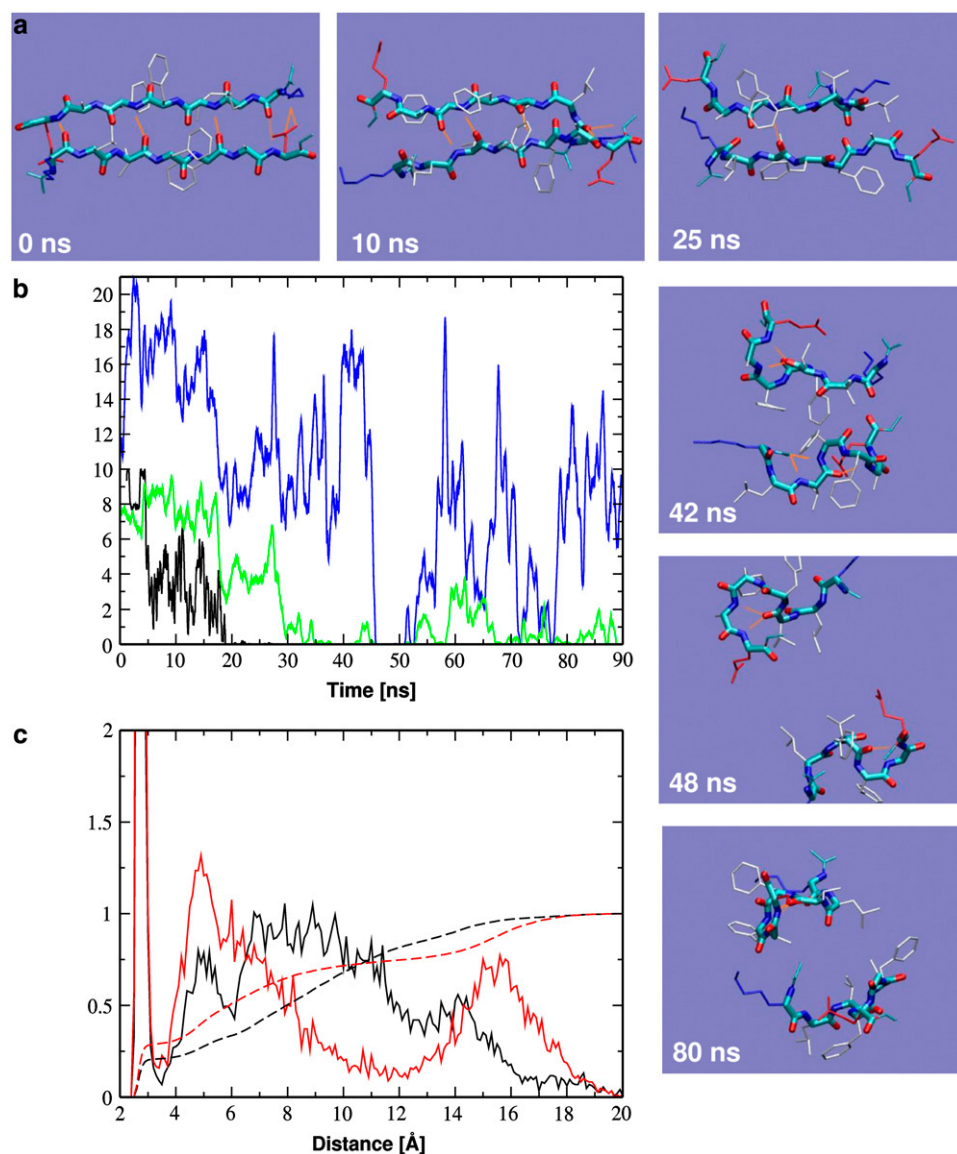

FIGURE 2 Dimer. (a) Snapshots of structures sampled during the simulation $\mathbf{2}_{300}$. Hydrophobic side chains are shown in white, Lys side chains in blue, Glu side chains in red, hydrogen bonds in orange. (b) β-sheet content (black, number of residues); polar contacts (green), hydrophobic contacts (blue). (c) Salt bridges between Lys[1] and Glu[14] (black) and between Glu[7] and Lys[8] (red) over the first 30 ns of the simulation. The histograms of the minimal distance between the charged groups are shown as full lines, while the integrals are shown as broken lines.

separated. Later they come closer again and are bound by fluctuating hydrophobic and polar interactions. This is probably due to the artificially high concentration in the simulation cell. At experimental dilution one may expect that the two peptides diffuse apart.

A detailed analysis of the breaking of the backbone-backbone hydrogen bonds present in the initial β-sheet structure reveals that the two most stable bonds (Val^{3}NH-Phe^{14}O and Val^{3}O-Phe^{14}NH) are very well shielded from the solvent by the hydrophobic Val and Phe side chains. Between 28.2 and 28.4 ns all atoms involved in the hydrogen bonds become partly exposed to solvent, which triggers the simultaneous breaking of the hydrogen bonds at 28.58 ns. This finding is in agreement with the idea that the formation and stability of backbone-backbone hydrogen bonds depend on their exposure to the solvent (66–68).

During the lifetime of the ordered dimer (first 30 ns of the simulation), the two possible salt bridges between the peptides (Lys^1-Glu^{14} and Glu^7-Lys^8) are formed, respectively, for 29% (Lys^1-Glu^{14}) and 21% (Glu^7-Lys^8) of the time (minimal distance between the charged groups <3.5 Å, Fig. 2 c). For an additional 21% and 13% of the time, respectively, the salt bridges are mediated by a water molecule (distance <6 Å, Fig. 2 c). These findings suggest that 1), electrostatic interactions between the peptides are present but not essential for the formation of a β-sheet; and 2), explicit modeling of water molecules is crucial for capturing this effect.

Single peptides have been simulated before and shown to be predominantly in a random coil structure (33,47). Our simulation shows that this tendency cannot be counterbalanced by the interaction between two peptides alone, probably because the backbone hydrogen bonds cannot be shielded effectively from the solvent and there is a insufficient number of hydrophobic contacts. This finding is in agreement with a recent parallel tempering MD study of the same peptide (69), where the authors find six different metastable dimer structures at 310 K, most of them in disordered conformations.

Since the β-sheet dimer is metastable for several nanoseconds, it could be assumed to be the minimal building block for β-sheet assembly. Experimental evidence points to the fact that different fibril-forming peptides, such as the very similar Aβ₁₄₋₂₃, also form stable dimers and/or tetramers (70). In case of Aβ₁₆₋₂₂ this mechanism could be additionally favored by the pairing of opposite charges in an antiparallel β-sheet dimer. We test this hypothesis in the following simulations.

Trimer

A similar disruption process as in case of the dimer is also seen for the trimer (Fig. 3). However, the disruption takes place on an even longer timescale.

The aggregate is more stable and one peptide loses its contact with the other two peptides after ∼70 ns only. Until this time the remaining two peptides stay paired in a β-structure.

We expect that if the simulation had been continued the two remaining peptides would also eventually dissociate, as is the case for the dimer.

Out of four possible salt bridges in the trimeric β-sheet, only one is highly populated (direct bridge for 44%, water-mediated bridge for 27% of the simulated time; see Fig. 3 c). It is situated between the two remaining peptides, suggesting that it contributes to the higher stability of the aggregate in this location.

MD simulations performed on the Aβ₁₆₋₂₂ trimer by other groups (33,48) demonstrate that an antiparallel β-sheet can be formed but shows large structural fluctuations. Full structural order in the aggregates requires a larger number of peptides, in agreement with our results. Interestingly, a study using a coarse-grained model finds a preference for an antiparallel orientation of the peptides despite ignoring the electrostatic interactions between the Lys and Glu side chains (47), suggesting that salt bridges are not crucial for β-sheet formation in agreement with our simulations.

Tetramer

Several simulations of four peptides were performed to help us understand whether a dimer is the minimal metastable building block of β-sheets, as the simulations of the dimer and the trimer seem to suggest. Different temperatures as well as different arrangements of four peptides were tested: a single-layered structure of four peptides in one antiparallel sheet (**4**₃₀₀ and **4**₃₄₈, Fig. 4 a), and a double-layered structure of two antiparallel sheets stacked on to each other (**4**₃₀₀/**PAR**$_{mixed}$ and **4**₃₄₈/**PAR**$_{mixed}$, Fig. 4 b).

At 300 K, the single sheet of four peptides does not break in 50 ns. The outer two peptides lose to a large extent their initial β-content, while the inner two peptides preserve their structure. Representative structures observed during the simulation are shown in Fig. 4 a.

At higher temperature (348 K), the sheet divides into a 2 × 2 arrangement after 13 ns, forming for a short time approximately an antiparallel stack of two antiparallel sheets. All β-content is completely lost after 40 ns, but during the simulated time of 70 ns only one peptide ever detaches completely from all the others.

In the 2 × 2 arrangement (Fig. 4 b), the four peptides remain together for the simulated time of 20 ns at 300 K, but the initial structure is not preserved. Instead, the two sheets rotate by ∼90° with respect to each other. The β-content is still 4.5 residues per peptide after 20 ns. Interestingly, the solvent-exposed hydrophobic surface does not increase during the rotation, since the side chains at the interface suitably adjust during this motion. In addition, there are two new hydrogen bonds formed between the backbone of initially opposed peptides.

In a longer simulation at higher temperature (**4**₃₄₈/**PAR**$_{mixed}$, 100 ns) starting from the same initial conformation, the same rotation is observed, but it occurs in a shorter
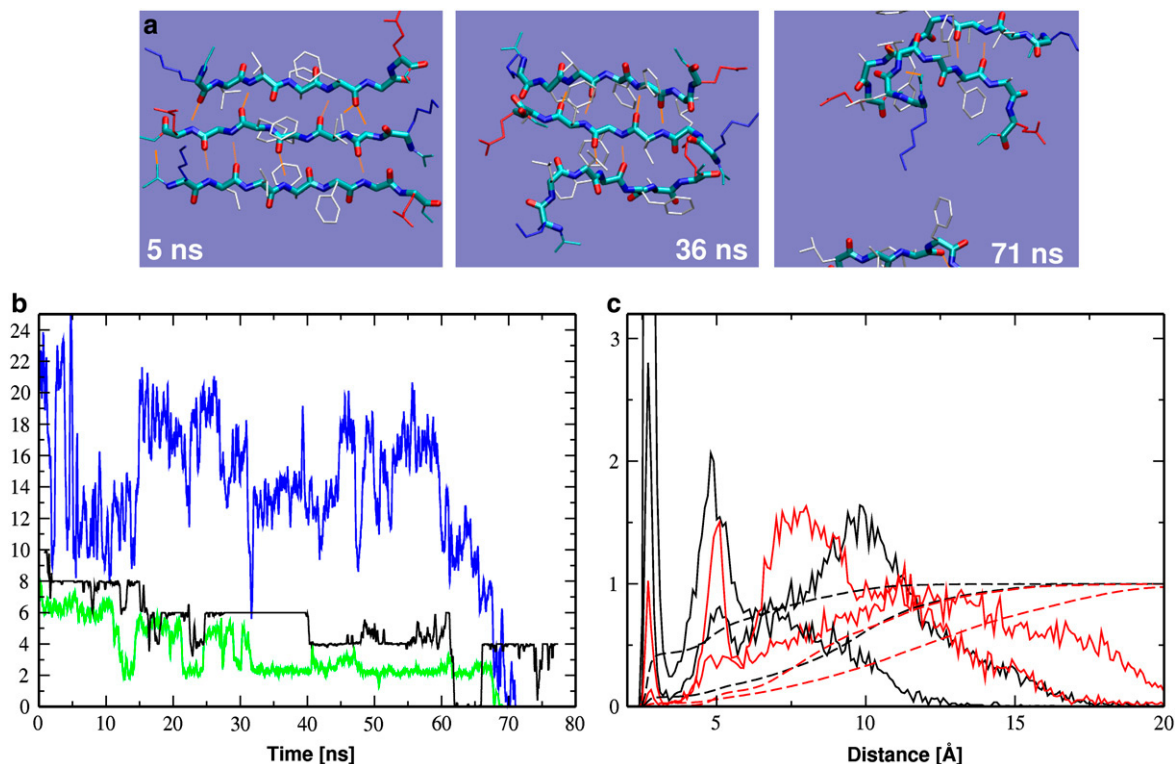
FIGURE 3   Trimer. (*a*) Snapshots of structures sampled during the simulation 3_{300} (same color-code as in Fig. 2). (*b*) β-sheet content of the two remaining peptides (*black*, number of residues); polar contacts of the detaching peptide (*green*), hydrophobic contacts of the detaching peptide (*blue*). (*c*) Salt bridges between peptide 1 and 2 (*black*) and between peptide 2 and 3 (*red*). The histograms of the minimal distance between the charged groups are given as full lines, while the integrals are given as broken lines.

time. While one of the sheets preserves roughly its initial structure and never breaks up, the other two peptides lose their β-content and both detach completely for a few hundred picoseconds from all other peptides. For most of the simulated time, they keep contact with the other sheet in a disordered fashion. The sampled conformations look similar to those of the simulations starting from one single sheet of four peptides (Fig. 4 *a*).

It could be postulated that the observed rotation is due to the electrostatic repulsion between the charged Lys and Glu side chains of opposite peptides, which are aligned in the parallel stacking. To test this hypothesis, we also simulated an antiparallel stacked assembly of two antiparallel sheets ($4_{300}/\text{AP}_{\text{mixed}}$). Here, the same characteristic rotation is observed, which suggests that it is not due to electrostatic effects. Analysis of the SASA suggests instead that the rotation increases the solvent exposure of the charged Lys and Glu side chains and at the same time lowers the solvent exposure of the less polar backbones.

In summary, we do not find a stable ordered β-sheet aggregate of four peptides, but the aggregates hardly ever break up, even on the 100-ns timescale at high temperature. The single-layered geometry seems to have an energy comparable to that of the double-layered geometry. Both arrangements display the same amount of hydrophobic surface.

In MD studies of different small amyloidogenic peptides, similar equilibria between single-layer and double-layer geometries have been observed (40,47,71), pointing to the fact that for an oligomer of this size both conformations are metastable, and the barrier for converting from one to the other is low. We will discuss the effect of different numbers of layers in more detail in Conclusions.

The hypothesis that the basic structural unit is a β-sheet of two peptides is not valid, since we also observe detachments of single peptides. Therefore, a more complex and cooperative interaction between the β-strands must be assumed.

Octamer

To test whether, for larger oligomers, a single-layer and a double-layer geometry are still comparably stable, we simulated different arrangements of the twofold-larger system.

We find that a single-layer geometry of eight peptides (8_{348}) is not stable. It starts twisting and later arranges in an approximately double-layered structure of four peptides in each sheet. During this process the β-content, the number of backbone-backbone hydrogen bonds, and the number of salt bridges decrease.

A double-layered parallel stack of antiparallel sheets was also probed. At 300 K ($8_{300}/\text{PAR}_{\text{mixed}}$), this conformation is

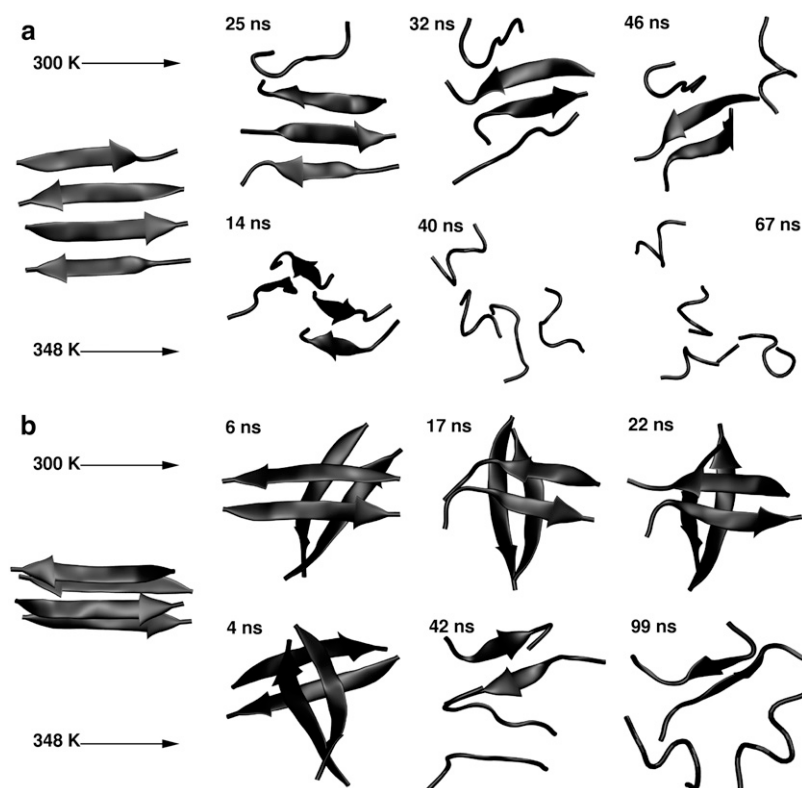FIGURE 4 Tetramer. Representative conformations from MD simulations. (*a*) Simulations starting from one sheet of four strands ($\mathbf{4}_{300}$ and $\mathbf{4}_{348}$). (*b*) Simulations starting from a 2 × 2 arrangement ($\mathbf{4}_{300}$/**PAR**$_{\mathrm{mixed}}$ and $\mathbf{4}_{348}$/**PAR**$_{\mathrm{mixed}}$).

very stable, showing only a small rotation of one sheet with respect to the other.

At higher temperature (348 K, $\mathbf{8}_{348}$/**PAR**$_{\mathrm{mixed}}$), we still observe a rotation of one sheet with respect to the other by ~90°. This is possible without major disruption of hydrophobic contacts, because the hydrophobic surface of a sheet of four Aβ_{16-22} peptides is roughly a square with a side length of 15 Å. Interestingly, during that rotation neither the polar nor the hydrophobic SASA changes. At the end of the simulation the β-content still amounts on average to four residues per peptide.

In summary, for the octamer the most stable among the investigated structures is a two-layered β-sheet geometry with four peptides in each sheet. This is different from the case of the tetramer, where the 2 × 2 structure has a stability comparable to the 1 × 4 structure.

The finding of an unstable single-layered octamer structure is at variance with the case of the amyloidogenic DFNKF peptide, where a stable single-layer nine-stranded β-sheet has been found in simulations (39). The difference can be explained by the higher hydrophilicity of this peptide, which disfavors the screening of side chains from the solvent at the interface of two sheets.

At 300 K the initial two-layered structure is stable during the simulation time. However, eight peptides still seem to be too few to form a well-aligned stacked β-sheet structure at higher temperature. We therefore probe a twofold-larger assembly, composed of two sheets of eight peptides each,

where the observed rotation should be hindered by the arrangement of the hydrophobic side chains.

16-mer

Based on the results on the stability of the smaller aggregates, in the present section we will assess the stability of aggregates of 16 Aβ_{16-22} peptides arranged in a two-layered β-sheet structure. In addition we will investigate the structural influence of different intersheet stacking modes (Fig. 1).

PAR$_{mixed}$

In simulation $\mathbf{16}_{300}$/**PAR**$_{\mathrm{mixed}}$, the β-structure of all peptides is very well conserved over the entire simulation length (Fig. 5 *a*). A small structural relaxation can be observed after 18 ns, when the aggregate disposes of some initial deformation acquired during the equilibration phase and assumes an almost perfectly aligned and flat β-sheet structure. After this event, the RMSD of the inner eight peptides from their average position is very low (0.72 ± 0.10 Å). The outer eight peptides are more flexible (RMSD 1.09 ± 0.19 Å) but also stable.

A striking feature of the β-sheet structure is that water is completely excluded from the interface between the two sheets (Fig. 5, *b* and *c*), which is formed by hydrophobic side-chain contacts. There are two water channels between the sheets, close to the polar side chains at the end of the peptides.
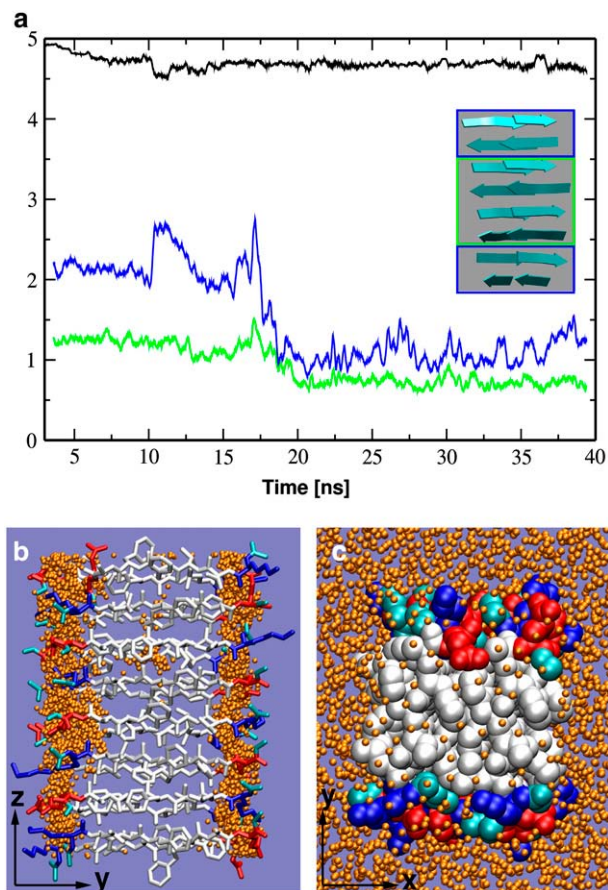
FIGURE 5 Simulation $\mathbf{16}_{300}/\mathbf{PAR}_{KVFE}$. (*a*) β-sheet content (*black*, number of residues per peptide), RMSD of inner eight peptides (*green*, Å), and RMSD of outer eight peptides (*blue*) with respect to the average structure of the last 20 ns. (*b*) Water channels inside the aggregate during the simulation (water positions taken from 200 snapshots, sampling interval of 10 ps). Water shown in orange, hydrophobic residues in white, Lys in blue, Glu in red; hydrogens omitted for clarity. (*c*) One snapshot of the simulation, showing that the Aβ_{16-22} peptides form a compact hydrophobic core. Same color code as in panel *b*.

Similar channels that serve to solvate buried polar side chains have been observed in simulations of Aβ_{9-40} (45).

On average there are 81 interbackbone hydrogen bonds, equivalent to 5.8 hydrogen bonds between each pair of neigh-

boring peptides. This corresponds almost to the value of the starting structure (6). On the other hand there are relatively few salt bridges present, eight on average, one of them between the two sheets.

To confirm our observation that this assembly of 16 peptides is stable, we also carried out a simulation at 348 K. Here the structure is very stable as well and moreover, close to the average structure observed at 300 K. The backbone RMSD between the converged average structures amounts to 0.8 Å only.

In summary, the simulated assembly of 16 peptides displays a very high stability. While the intrasheet interactions include backbone-hydrogen bonds and side-chain hydrophobic contacts, the main intersheet interactions are exclusively hydrophobic contacts.

PAR$_{LFA}$ and AP$_{LFA}$

Two simulations have been carried out for two sheets stacked together by the LFA-LFA interface, one with a parallel stacking ($\mathbf{16}_{300}/\mathbf{PAR}_{LFA}$) and one with an antiparallel stacking ($\mathbf{16}_{300}/\mathbf{AP}_{LFA}$). The detachment of a peptide is never observed, and the β-sheet structure is largely preserved.

However, both structures show a stronger deviation from a perfectly aligned, planar β-sheet structure than $\mathbf{16}_{300}/\mathbf{PAR}_{mixed}$. In $\mathbf{16}_{300}/\mathbf{PAR}_{LFA}$, two collective movements can be distinguished (Fig. 6): a slight twisting of the sheets; and a small shift in z direction of one sheet with respect to the other. The structure is not yet converged after 25 ns of simulation. In $\mathbf{16}_{300}/\mathbf{AP}_{LFA}$ on the other hand, a very twisted structure (Fig. 6 *a*) is quickly formed within 3 ns and stable for the rest of the simulation, which suggests that a stable minimum has been reached.

The collective movements of the sheets can be understood by looking at their interactions. Since the charged amino acids are pointing outwards and are well solvated by water, the intersheet contacts are limited to three hydrophobic side chains (Leu, Phe, Ala). The sheet distance has a lower bound of ~10 Å imposed by the bulky phenyl rings. However, at this distance the small Ala side chains cannot form good contacts. The twisting and shifting of the sheets helps to
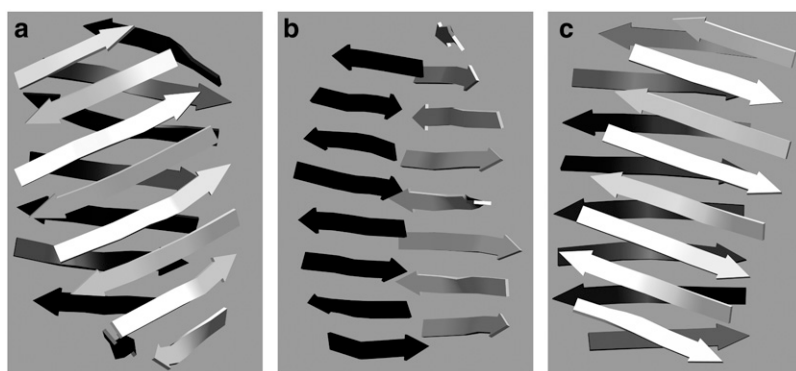

FIGURE 6 Rearrangements of β-sheets with different stackings. (*a*) Twist of sheets (observed in $\mathbf{16}_{300}/\mathbf{AP}_{LFA}$), (*b*) shift in z direction by one peptide (observed in $\mathbf{16}_{300}/\mathbf{PAR}_{LFA}$), and (*c*) rotation of one sheet with respect to the second sheet (observed in $\mathbf{16}_{300}/\mathbf{PAR}_{KVFE}$).

ensure a better hydrophobic contact, which is confirmed by the decrease of the hydrophobic SASA during the initial movements.

PAR$_{KVFE}$

Simulation 16_{300}/PAR$_{KVFE}$ initially displays some rotation of one sheet with respect to the other (Fig. 6 c) and a shift of half a peptide's width in the z direction, but it converges slowly (in ~18 ns) to a structure similar to 16_{300}/PAR$_{mixed}$, i.e., without twists, rotations, or shifts. This simulation shows the highest number of salt bridges between the charged Lys and Glu side chains. On average there are 12 intrasheet and 11 intersheet salt bridges, with some residues forming more than one salt bridge. Due to this partial burial of the charged groups, 16_{300}/PAR$_{KVFE}$ also displays the lowest polar and the lowest total SASA. However, it displays at the same time the highest hydrophobic SASA of all tested stackings. The corners of the aggregate are slightly disordered because of the preference of the charged side chains to interact with water. Good hydrophobic contacts between the sheets are assured through Phe-Phe and Val-Val interactions.

Stability and sheet stacking

In summary, all of the tested β-sheet aggregates of 16 peptides are stable, and no detachment or loss of β-conformation is observed, not even at elevated temperature. However, different intersheet stackings can result in aggregates with different quaternary structures.

Convergence of large-scale movements like the twisting, shifting, and rotating of large β-sheets is slow on the MD timescale. Nevertheless, our simulations suggest that PAR$_{mixed}$ and PAR$_{KVFE}$ form flat and well-aligned aggregates, while PAR$_{LFA}$ and AP$_{LFA}$ form twisted structures to ensure optimal intersheet contacts. More specifically, a left-handed helical twist is observed in both simulations. The sense of the twist is in agreement with the twists found experimentally in amyloid fibrils formed by different peptides (72–75).

While PAR$_{KVFE}$ has the lowest total SASA, it displays the highest hydrophobic SASA of all 16-mers. PAR$_{mixed}$, on the other hand, shows the lowest hydrophobic SASA. The best shielding of the backbone from the solvent is observed in PAR$_{LFA}$, which displays also the lowest potential energy. Here, good shielding is provided by the KVFE side chains pointing outside to the solvent on both outer surfaces.

In case of much longer fibrils, the rotational movement observed in PAR$_{KVFE}$ should be further inhibited, while shifting along the z axis should be facilitated. In this manner, a fast transformation between parallel and antiparallel stackings is possible.

For restrictions in computational time we have not simulated the 16-mer with AP$_{mixed}$ and AP$_{KVFE}$ stackings. However, based on the observation that a shift in z direction can occur spontaneously, transforming a parallel stacking into an antiparallel stacking, and on the observation that PAR$_{LFA}$ and AP$_{LFA}$ behave similarly, we would expect that also AP$_{mixed}$ and AP$_{KVFE}$ would form flat and well-aligned aggregates.

32-mer

If more than two sheets are stacked together, combinations of different stacking modes are possible. The only periodically repeatable stacking is PAR$_{mixed}$ (or AP$_{mixed}$). A simulation of four sheets in PAR$_{mixed}$ stacking (32_{300}/PAR$_{mixed}$) was carried out. The aggregate is very stable with all peptides staying in β-conformation. The only observable large-scale movement is a rotation of one external sheet (sheet IV, Fig. 7 a) with respect to the other three sheets. This relaxation is completed within 10 ns and stable for the following 25 ns (RMSD in Fig. 7 c). It should be noted that the other three sheets, which interact through the same interface as the
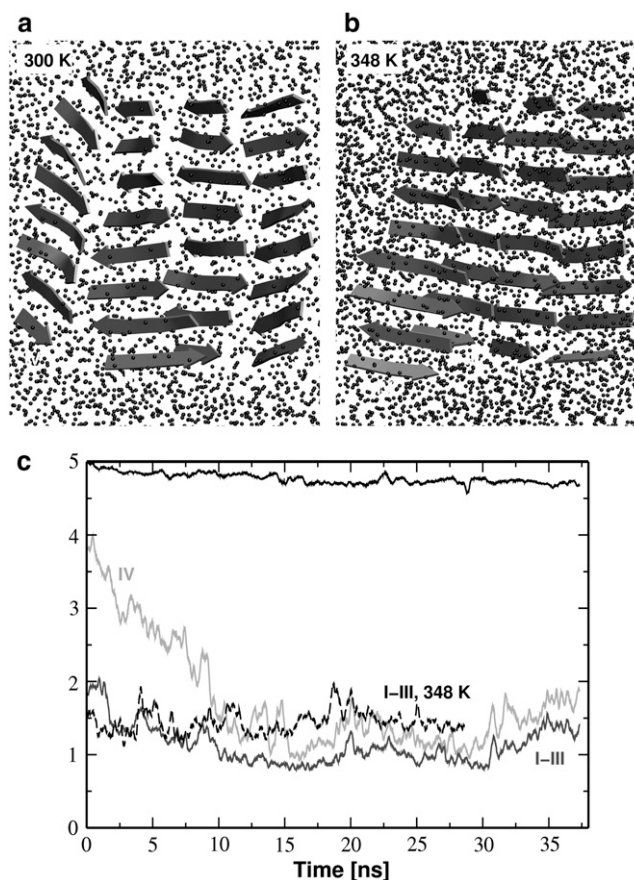

FIGURE 7   32-mer. (a) Snapshot from simulation 32_{300}/PAR$_{mixed}$. (b) Snapshot from simulation 32_{348}/PAR$_{mixed}$. (c) β-sheet content (solid line, number of residues per peptide) and RMSD from the average structure of sheets I–III during the last 27-ns of simulation 32_{300}/PAR$_{mixed}$ (in Å). Sheets I–III (dark shaded line), sheet IV (light shaded line), and sheets I–III from 32_{348}/PAR$_{mixed}$ (dashed line).

rotated sheet, remain completely flat and aligned, suggesting that the rotation is due to equilibration of the initial structure. On average, there are 18 salt bridges present, roughly four per sheet and two between two sheets.

Starting from the final structure of simulation 32_{300}/$\mathbf{PAR}_{mixed}$, another simulation was carried out at 348 K (32_{348}/$\mathbf{PAR}_{mixed}$). Within the simulated 30 ns, sheet *IV* rotates back, so that the peptide backbones are again aligned with the *y* axis, but it remains shifted by one peptide in *z* direction (Fig. 7 *b*). Again, the structure of sheets *I–III* remains completely flat and aligned as at 300 K, suggesting that this part of the aggregate is well equilibrated and stable.

We have calculated the trajectory average of the x-ray diffraction pattern of the 32-mer system according to Eqs. 3 and 4. In Fig. 8 *a*, the characteristic cross-β pattern of amyloid fibrils is observed. By plotting separately the meridional and the equatorial x-ray diffraction pattern (Fig. 8 *b*), we can confirm that the peak at 4.9 Å originates from the inter-peptide distance (*z* direction), while the peak at 11.1 Å stems from the intersheet distance (*x* direction). We obtain slightly smaller distances when calculating the x-ray diffraction pattern of a larger β-sheet model (data not shown), pointing to a finite size effect.
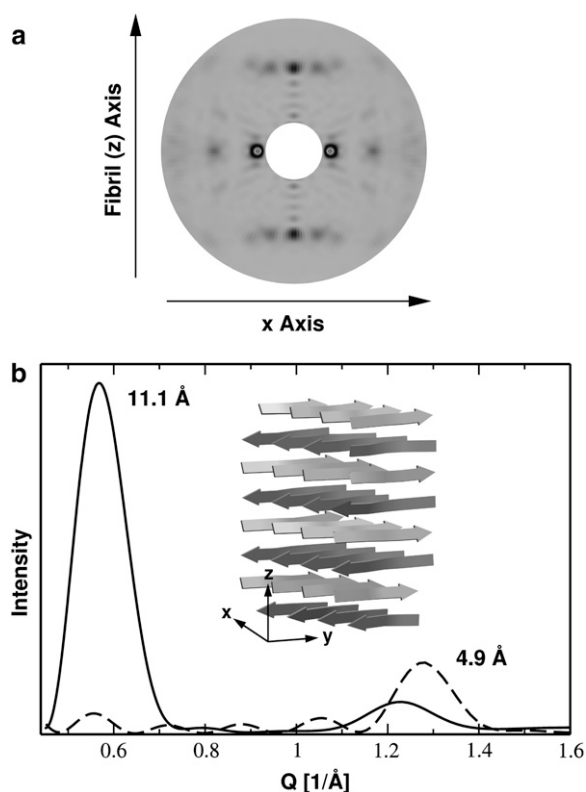

FIGURE 8 (*a*) Calculated x-ray diffraction pattern of the 32-mer, averaged over the last 26 ns of simulation 32_{300}/$\mathbf{PAR}_{mixed}$ (26 frames, sampling time 1 ns). (*b*) Equatorial (*solid line*) and meridional (*dashed line*) x-ray diffraction pattern extracted from the same calculation. The equatorial peak reflects the intersheet distance, while the meridional peak reflects the interpeptide distance.

To our knowledge the only x-ray diffraction data available for A$\beta_{16–22}$ has been recorded in a lyophilized powder and displays periodicities of 4.7 and 9.9 Å (46). The latter is smaller than the typical intersheet distances (10.6 Å) in a number of Alzheimer-related peptides (13,14,16,76). How-ever, it has been found that the intersheet distance measured by x-ray diffraction depends crucially on sample preparation: for different fragments of A$\beta_{1–42}$, the distance between lyophilized, vapor-hydrated, and dried fibrils can vary by as much as 3 Å for the same system (77).

In summary, the calculated x-ray diffraction pattern is in good agreement with experimental data and suggests that our model is similar to the structures found in vitro.

CONCLUSIONS

The present large-scale explicit-solvent MD simulations yield insight into the properties of A$\beta_{16–22}$ oligomers of 2–32 peptides. Oligomers of this size are believed to play a crucial role in the Alzheimer pathology (10).

A result from our simulations, which is in agreement with earlier studies (39,78) and with experimental evidence, is that the β-sheet aggregates are stable only if larger than a critical size. While a β-sheet dimer breaks up after a few tens of nanoseconds, the trimer and tetramer take a significantly longer time, and higher oligomers are stable during the course of the simulations. Assemblies of eight peptides are gener-ally stable but show some structural flexibility. The biggest tested assemblies of 16 and 32 peptides show very high struc-tural stability. We attribute this to better hydrophobic contacts and a better shielding of backbone-backbone hydrogen bonds from the solvent, which is possible in larger assemblies. Electrostatic effects seem to play a secondary role for the stability of the aggregates, as suggested by the relatively few salt bridges between the charged Glu and Lys side chains. Very stable structures (e.g., in 16_{300}/$\mathbf{PAR}_{mixed}$) are observed, where only ~50% of the possible salt bridges are formed. However, electrostatic effects may play a crucial role for the aggregation process (30).

In Fig. 9 we plot the total SASA observed in our simu-lations as a function of the number of peptides. It can be seen that for a given number of β-sheet layers, the SASA depends linearly on the number of peptides. While the *y* axis intercept increases with the number of layers, the slope decreases with the number of layers. This behavior can be qualitatively explained by a simple geometrical model, considering each peptide as a parallelepiped, as it is sketched in the inset of Fig. 9 for the case of eight peptides. Each sheet has two exposed surfaces in the *x,y* plane, regardless of the number of peptides in the sheet. While the number of exposed surfaces in the *y,z* plane depends linearly on the number of peptides and inversely linearly on the number of sheets, the number of exposed surfaces in the *x,z* plane depends solely and linearly on the number of peptides.
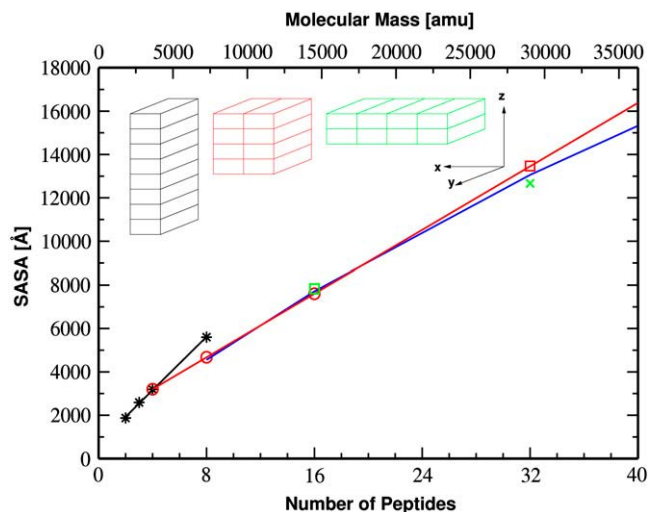
FIGURE 9 Total SASA (in Å^2) as a function of the number of peptides. The data points are extracted from the MD simulations, and linear fits are displayed for the single-layered (*black*) and double-layered (*red*, **PAR**$_{\text{mixed}}$ stacking) structures. For the four-layered structure (*green*) only one long simulation has been performed. The SASA extracted from two short simulations of a 4 × 4 (*green square*) and of a 2 × 16 (*red square*) arrangement confirm our predictions. The blue curve corresponds to the empirical formula derived for oligomeric proteins (79).

In the case of four peptides, the observed SASA is the same for a single-layered and a double-layered arrangement. In the case of eight peptides, however, the observed SASA is significantly lower for a double-layered arrangement. This is in perfect agreement with the stabilities found in our simulations: while the tetramer samples both single-layered and double-layered conformations starting from either geometry, the octamer is only stable in a double-layered conformation.

To confirm our predictions, we carried out two additional short simulations of a 2 × 16 (Fig. 9, *red square*) and of a 4 × 4 (*green square*) arrangement. The value for the 2 × 16 structure lies exactly on the linear fit to the other points of a double-layered structure and is larger than the value of the 4 × 8 structure. The value obtained for the 4 × 4 structure is slightly larger than the one obtained for the 2 × 8 structure. Therefore the crossover from a more stable double-layered to a more stable four-layered structure is predicted to be between 16 and 32 peptides.

If we extrapolate these findings to a much larger number of peptides, we would conclude that a lateral growth of fibrils (in β-sheet stacking direction) should be favorable over a longitudinal growth (in hydrogen-bonding direction). This is obviously not true, but the experimentally observed formation of long fibrils containing only a few sheets can be explained by kinetic factors. It is known that dimer and oligomer formation is a slow process, while fibril growth from a preformed seed is a fast process. A preformed β-sheet aggregate can add monomers only in hydrogen-bonding direction, while the addition of another sheet is possible only by

adding a preformed oligomer. Therefore longitudinal growth is faster than lateral growth. On the other hand, it has recently been shown that amyloidogenic peptides can also form microcrystals with lateral dimensions of 12–240 nm (16,17), supporting our conclusion that lateral growth is energetically accessible.

Interestingly, the observed SASAs for the larger aggregates agree well with the empirical formula derived for the SASA of oligomeric proteins

$$\text{SASA} = 5.3 \times M^{0.76}, \tag{5}$$

where the surface is given in Å^2 and the molecular mass M in atomic mass units (79). However, the surface of the Aβ_{16-22} oligomers is more hydrophobic (72% in case of the dimer, 65% in case of the 32-mer) than the one of a globular protein.

There are six distinct possibilities to stack two in-register antiparallel sheets of Aβ_{16-22} on to each other. Depending on the interface, we observe straight or twisted structures. Since mixtures of these stackings are unlikely within the same aggregate due to the symmetry of an antiparallel β-sheet, it can be assumed that in a seeded solution the stacking of the seed will be propagated. It could further be hypothesized that under neutral pH, **AP**$_{\text{LFA}}$, which displays a twisted structure, is more likely to form than **PAR**$_{\text{KVFE}}$, which displays a flat structure, because of the better solvation of the charged Lys and Glu side chains. This effect should be smaller under acidic or basic pH, where one of the side chains would be neutralized, so that the formation of **PAR**$_{\text{KVFE}}$ becomes more likely. We therefore propose that the stacking of different interfaces could be related to different fibril morphologies found in vitro at different pH. A similar suggestion has been made for the case of the Aβ_{1-40} peptide (52).

We calculated the x-ray diffraction pattern of our biggest system (32-mer) to compare our data directly to the available experimental data. We observe peaks signaling periodicities that are close to the corresponding experimental determinations. In view of this agreement we assume that the simulated structures are very similar to the experimental ones.

REFERENCES

1. Dobson, C. 2002. Getting out of shape. *Nature*. 418:729–730.

2. Dobson, C. 2003. Protein folding and misfolding. *Nature*. 426:884–890.

3. Selkoe, D. J. 2003. Folding proteins in fatal ways. *Nature*. 426:900–904.

4. Lorenzo, A., and B. A. Yanker. 1994. β-amyloid neurotoxicity requires fibril formation and is inhibited by Congo red. *Proc. Natl. Acad. Sci. USA*. 91:12243–12247.

5. Klein, W. L. 2002. Aβ toxicity in Alzheimer's disease: globular oligomers (ADDLs) as new vaccine and drug targets. *Neurochem. Int.* 41:345–352.

6. Hardy, J., and D. J. Selkoe. 2002. The amyloid hypothesis of Alzheimer's disease: progress and problems on the road to therapeutics. *Science*. 297:353–356.

7. Bucciantini, M., E. Giannoni, F. Chiti, F. Baroni, L. Formigli, J. S. Zurdo, N. Taddei, G. Ramponi, C. M. Dobson, and M. Stefani. 2002. Inherent toxicity of aggregates implies a common mechanism for protein misfolding diseases. *Nature*. 416:507–511.

8. Bucciantini, M., G. Calloni, F. Chiti, L. Formigli, D. Nosi, C. M. Dobson, and M. Stefani. 2004. Prefibrillar amyloid protein aggregates share common features of cytotoxicity. *J. Biol. Chem.* 279:31374–31382.

9. Bernstein, S. L., T. Wyttenbach, A. Baumketner, J.-E. Shea, D. B. Teplow, and M. T. Bowers. 2005. Amyloid β-protein: monomer structure and early aggregation states of Aβ42 and its Pro[19] alloform. *J. Am. Chem. Soc.* 127:2075–2084.

10. Lesné, S., M. Teng Koh, L. Kotilinek, R. Kayed, C. G. Glabe, A. Yang, M. Gallagher, and K. H. Ashe. 2006. A specific amyloid-β protein assembly in the brain impairs memory. *Nature*. 440:352–357.

11. Scheibl, T., R. Parthasarathy, G. Sawicki, X.-M. Lin, H. Jaeger, and S. L. Lindquist. 2003. Conducting nanowires built by controlled self-assembly of amyloid fibers and selective metal deposition. *Proc. Natl. Acad. Sci. USA*. 100:4527–4532.

12. Reches, M., and E. Gazit. 2003. Casting metal nanowires within discrete self-assembled peptide nanotubes. *Science*. 300:625–627.

13. Kirschner, D. A., C. Abraham, and D. J. Selkoe. 1986. X-ray diffraction from intraneuronal paired helical filaments and extraneuronal amyloid fibers in Alzheimer disease indicates cross-β conformation. *Proc. Natl. Acad. Sci. USA*. 83:503–507.

14. Kirschner, D. A., H. Inouye, L. K. Duffy, A. Sinclair, M. Lind, and D. J. Selkoe. 1987. Synthetic peptide homologous to β protein from Alzheimer disease forms amyloid-like fibrils in vitro. *Proc. Natl. Acad. Sci. USA*. 84:6953–6957.

15. Sunde, M., L. C. Serpell, M. Bartlam, P. E. Fraser, M. B. Bepys, and C. C. F. Blake. 1997. Common core structure of amyloid fibrils by synchrotron x-ray diffraction. *J. Mol. Biol.* 273:729–739.

16. Makin, O. S., E. Atkins, P. Sikorski, J. Johansson, and L. C. Serpell. 2005. Molecular basis for amyloid fibril formation and stability. *Proc. Natl. Acad. Sci. USA*. 102:315–320.

17. Nelson, R., M. R. Sawaya, M. Balbirnie, A. O. Madsen, C. Riekel, R. Grothe, and D. Eisenberg. 2005. Structure of the cross-β spine of amyloid-like fibrils. *Nature*. 435:773–778.

18. Dzwolak, W., R. Jansen, V. Smirnovas, A. Loksztejn, S. Porowski, and R. Winter. 2005. Template-controlled conformational patterns of insulin fibrillar self-assembly reflect history of solvation of the amyloid nuclei. *Phys. Chem. Chem. Phys.* 7:1349–1351.

19. Gosal, W., I. J. Morten, E. W. Hewitt, D. A. Smith, N. H. Thomson, and S. E. Radford. 2005. Competing pathways determine fibril morphology in the self-assembly of β2-microglobulin into amyloid. *J. Mol. Biol.* 351:850–864.

20. Krishnan, R., and S. L. Lindquist. 2005. Structural insights into a yeast prion illuminate nucleation and strain diversity. *Nature*. 435:765–772.

21. Petkova, A. T., R. D. Leapman, Z. H. Guo, W. M. Yau, M. P. Mattson, and R. Tycko. 2005. Self-propagating, molecular-level polymorphism in Alzheimer's β-amyloid fibrils. *Science*. 307:262–265.

22. Lomakin, A., D. S. Chung, G. B. Benedek, D. A. Kirschner, and D. B. Teplow. 1996. On the nucleation and growth of amyloid β-protein fibrils: detection of nuclei and quantitation of rate constants. *Proc. Natl. Acad. Sci. USA*. 93:1125–1129.

23. Kelly, J. W. 1998. The alternative conformations of amyloidogenic proteins and their multi-step assembly pathways. *Curr. Opin. Struct. Biol.* 8:101–106.

24. Ban, T., M. Hoshino, S. Takahashi, D. Hamada, K. Hasegawa, H. Naiki, and Y. Goto. 2004. Direct observation of Aβ amyloid fibril growth and inhibition. *J. Mol. Biol.* 344:757–767.

25. Sabaté, R., M. Gallardo, and J. Estelrich. 2005. Temperature dependence of the nucleation constant rate in β amyloid fibrillogenesis. *Int. J. Biol. Macromol.* 35:9–13.

26. Carrotta, R., M. Manno, D. Bulone, V. Martorana, and P. L. San Biagio. 2005. Protofibril formation of amyloid β-protein at low pH via

a non-cooperative elongation mechanism. *J. Biol. Chem.* 280:30001–30008.

27. Carulla, N., G. L. Caddy, D. R. Hall, J. Zurdo, M. Gairi, M. Feliz, E. Giralt, C. V. Robinson, and C. M. Dobson. 2005. Molecular recycling within amyloid fibrils. *Nature*. 436:554–558.

28. Petty, S. A., and S. M. Decatur. 2005. Correlations among morphology, β-sheet stability, and molecular structure in prion peptide aggregates. *Proc. Natl. Acad. Sci. USA*. 102:14272–14277.

29. Petty, S. A., and S. M. Decatur. 2005. Experimental evidence for the reorganization of β-strands within aggregates of the Aβ16–22 peptide. *J. Am. Chem. Soc.* 127:13488–13489.

30. Tjernberg, L., W. Hosia, N. Bark, J. Thyberg, and J. Johansson. 2002. Charge attraction and β propensity are necessary for amyloid fibril formation from tetrapeptides. *J. Biol. Chem.* 277:43243–43246.

31. Li, L., T. A. Darden, L. Bartolotti, D. Kominos, and L. Pedersen. 1999. An atomic model for the pleated β-sheet structure of Aβ amyloid protofilaments. *Biophys. J.* 76:2871–2878.

32. Ma, B., and R. Nussinov. 2002. Stabilities and conformations of Alzheimer's β-amyloid peptide oligomers (Aβ16–22, Aβ16–35, and Aβ10–35): sequence effects. *Proc. Natl. Acad. Sci. USA*. 99:14126–14131.

33. Klimov, D. K., and D. Thirumalai. 2003. Dissecting the assembly of Aβ16–22 amyloid peptides into antiparallel β-sheets. *Structure*. 11:295–307.

34. Simona, F., G. Tiana, R. A. Broglia, and G. Colombo. 2004. Modeling the α-helix to β-hairpin transition mechanism and the formation of oligomeric aggregates of the fibrillogenic peptide Aβ12–28: insights from all-atom molecular dynamics simulations. *J. Mol. Graph. Model.* 23:263–273.

35. Tsai, H.-H. G., D. Zanuy, N. Haspel, K. Gunasekaran, B. Ma, C.-J. Tsa, and R. Nussinov. 2004. The stability and dynamics of the human calcitonin amyloid peptide DFNKF. *Biophys. J.* 87:146–158.

36. Zanuy, D., Y. Porat, E. Gazit, and R. Nussinov. 2004. Peptide sequence and amyloid formation: molecular simulations and experimental study of a human islet amyloid polypeptide fragment and its analogs. *Structure*. 12:439–455.

37. Cecchini, M., F. Rao, M. Seeber, and A. Caflisch. 2004. Replica exchange molecular dynamics simulations of amyloid peptide aggregation. *J. Chem. Phys.* 121:10748–10756.

38. Tarus, B., J. E. Straub, and D. Thirumalai. 2005. Probing the initial stage of aggregation of the Aβ10–35-protein: assessing the propensity for peptide dimerization. *J. Mol. Biol.* 345:1141–1156.

39. Haspel, N., D. Zanuy, B. Ma, H. Wolfson, and R. Nussinov. 2005. A comparative study of amyloid fibril formation by residues 15–19 of the human calcitonin hormone: a single β-sheet model with a small hydrophobic core. *J. Mol. Biol.* 345:1213–1227.

40. López de la Paz, M., G. M. S. de Mori, L. Serrano, and G. Colombo. 2005. Sequence dependence of amyloid fibril formation: insights from molecular dynamics simulations. *J. Mol. Biol.* 349:583–596.

41. Melquiond, A., G. Boucher, N. Mousseau, and P. Derreumaux. 2005. Following the aggregation of amyloid-forming peptides by computer simulations. *J. Chem. Phys.* 122:174904.

42. Soto, P., J. Cladera, A. E. Mark, and X. Daura. 2005. Stability of SIV gp32 fusion-peptide single-layer protofibrils as monitored by molecular-dynamics simulations. *Angew. Chem. Int. Ed. Engl.* 44:1065–1067.

43. Valerio, M., A. Colosimo, F. Conti, A. Giuliani, A. Grottesi, C. Manetti, and J. P. Zbilut. 2005. Early events in protein aggregation: molecular flexibility and hydrophobicity/charge interaction in amyloid peptides as studied by molecular dynamics simulations. *Proteins*. 58:110–118.

44. Wu, C., H. Lei, and Y. Duan. 2005. Elongation of ordered peptide aggregate of an amyloidogenic hexapeptide NFGAIL observed in molecular dynamics simulations with explicit solvent. *J. Am. Chem. Soc.* 127:13530–13537.

45. Buchete, N.-V., R. Tycko, and G. Hummer. 2005. Molecular dynamics simulations of Alzheimer's β-amyloid protofilaments. *J. Mol. Biol.* 353:804–821.

46. Balbach, J. J., Y. Ishii, O. N. Antzutkin, R. D. Leapman, N. W. Rizzo, F. Dyda, J. Reed, and R. Tycko. 2000. Amyloid fibril formation by Aβ_{16-22}, a seven-residue fragment of the Alzheimer's β-amyloid peptide, and structural characterization by solid state NMR. *Biochemistry.* 39:13748–13759.

47. Favrin, G., A. Irbäck, and S. Mohanty. 2004. Oligomerization of amyloid Aβ_{16-22} peptides using hydrogen bonds and hydrophobicity forces. *Biophys. J.* 87:3657–3664.

48. Santini, S., N. Mousseau, and P. Derreumaux. 2004. In silico assembly of Alzheimer's Aβ_{16-22} peptide into β-sheets. *J. Am. Chem. Soc.* 126:11509–11516.

49. Santini, S., G. Wei, N. Mousseau, and P. Derreumaux. 2004. Pathway complexity of Alzheimer's β-amyloid Aβ_{16-22} peptide assembly. *Structure.* 12:1245–1255.

50. Blake, C., and L. Serpell. 1996. Synchrotron x-ray studies suggest that the core of the transthyretin amyloid fibril is a continuous β-sheet helix. *Structure.* 4:989–998.

51. Burkroth, T. S., T. L. S. Benziger, V. Urban, D. M. Morgan, D. M. Gregory, P. Thiyagarajan, R. E. Botto, S. C. Meredith, and D. G. Lynn. 2000. Structure of the β-amyloid (10–35) fibril. *J. Am. Chem. Soc.* 122:7883–7889.

52. Petkova, A. T., W. M. Yau, and R. Tycko. 2006. Experimental constraints on quaternary structure in Alzheimer's β-amyloid fibrils. *Biochemistry.* 45:498–512.

53. Wang, J., P. Cieplak, and P. A. Kollman. 2000. How well does a restrained electrostatic potential (RESP) model perform in calculating conformational energies of organic and biological molecules? *J. Comput. Chem.* 21:1049–1074.

54. Jorgensen, W. L., J. Chandrasekhar, J. D. Madura, R. W. Impey, and M. L. Klein. 1983. Comparison of simple potential functions for simulating liquid water. *J. Chem. Phys.* 79:926–935.

55. Berendsen, H. J. C., D. van der Spoel, and R. van Drunen. 1995. GROMACS—a message-passing parallel molecular-dynamics implementation. *Comput. Phys. Commun.* 91:43–56.

56. Lindahl, E., B. Hess, and D. van der Spoel. 2001. GROMACS 3.0: a package for molecular simulation and trajectory analysis. *J. Mol. Model. (Online).* 7:306–317.

57. van der Spoel, D., E. Lindahl, B. Hess, G. Groenhof, A. E. Mark, and H. J. C. Berendsen. 2005. GROMACS: fast, flexible, and free. *J. Comput. Chem.* 26:1701–1718.

58. Essman, U., L. Perera, M. L. Berkowitz, T. A. Darden, H. Lee, and L. G. Pedersen. 1995. A smooth particle-mesh Ewald method. *J. Chem. Phys.* 103:8577–8593.

59. Hess, B., H. Bekker, H. J. C. Berendsen, and J. G. E. M. Fraaije. 1997. LINCS: a linear constraint solver for molecular simulations. *J. Comput. Chem.* 18:1463–1472.

60. Berendsen, H. J. C., J. P. M. Postma, W. F. V. Gunsteren, A. DiNola, and J. R. Haak. 1984. Molecular dynamics with coupling to an external bath. *J. Chem. Phys.* 81:3684–3690.

61. Kabsch, W., and C. Sander. 1983. Dictionary of protein secondary structure: pattern recognition of hydrogen-bonded and geometrical features. *Biopolymers.* 22:2577–2637.

62. Tsodikov, O. V., M. T. Record, Jr., and Y. V. Sergeev. 2002. Novel computer program for fast exact calculation of accessible and molecular surface areas and average surface curvature. *J. Comput. Chem.* 23:600–609.

63. Richards, F. M. 1977. Areas, volumes, packing, and protein structure. *Annu. Rev. Biophys. Bioeng.* 6:151–176.

64. Chantler, C. T. 1995. Theoretical form-factor, attenuation and scattering tabulation for $z = 1–92$ from $e = 1–10 eV$ to $e = 0.4–1.0 meV$. *J. Phys. Chem. Ref. Data.* 24:71–643.

65. Chantler, C. T. 2000. Detailed tabulation of atomic form factors, photoelectric absorption and scattering cross section, and mass attenuation coefficients in the vicinity of absorption edges in the soft x-ray ($z = 30–36$, $z = 60–89$, $e = 0.1 keV–10 keV$), addressing convergence issues of earlier work. *J. Phys. Chem. Ref. Data.* 29:597–1048.

66. García, A. E., and K. Y. Sanbonmatsu. 2002. α-helical stabilization by side chain shielding of backbone hydrogen bonds. *Proc. Natl. Acad. Sci. USA.* 99:2782–2787.

67. Fernández, A., J. Kardos, L. R. Scott, Y. Goto, and R. S. Berry. 2003. Structural defects and the diagnosis of amyloidogenic propensity. *Proc. Natl. Acad. Sci. USA.* 100:6446–6451.

68. Fernández, A. 2005. What factor drives the fibrillogenic association of β-sheets? *FEBS Lett.* 579:6635–6640.

69. Gnanakaran, S., R. Nussinov, and A. E. García. 2006. Atomic-level description of amyloid β-dimer formation. *J. Am. Chem. Soc.* 128:2158–2159.

70. Tjernberg, L., D. J. E. Callaway, A. Tjernberg, S. Hahne, C. Lilliehöök, L. Terenius, J. Thyberg, and C. Nordstedt. 1999. A molecular model of Alzheimer amyloid β-peptide fibril formation. *J. Biol. Chem.* 274:12619–12625.

71. Wei, G., N. Mousseau, and P. Derreumaux. 2004. Sampling the self-assembly pathways of KFFE hexamers. *Biophys. J.* 87:3648–3656.

72. Jiménez, J. L., E. J. Nettleton, M. Bouchard, C. V. Robinson, C. M. Dobson, and H. R. Salbil. 2002. The protofilament structure of insulin amyloid fibrils. *Proc. Natl. Acad. Sci. USA.* 99:9196–9201.

73. Goldsbury, C., P. Frey, V. Olivieri, U. Aebi, and S. A. Müller. 2005. Multiple assembly pathways underlie amyloid-β fibril polymorphisms. *J. Mol. Biol.* 352:282–298.

74. Saiki, M., S. Honda, K. Kawasaki, D. Zhou, A. Kaito, T. Konakahara, and H. Morii. 2005. Higher-order molecular packing in amyloid-like fibrils constructed with linear arrangements of hydrophobic and hydrogen-bonding side-chains. *J. Mol. Biol.* 348:983–998.

75. Kanno, T., K. Yamaguchi, H. Naiki, Y. Goto, and T. Kawai. 2005. Association of thin filaments into thick filaments revealing the structural hierarchy of amyloid fibrils. *J. Struct. Biol.* 149:213–218.

76. Sikorski, P., E. D. T. Atkins, and L. C. Serpell. 2003. Structure and texture of fibrous crystals formed by Alzheimer's Aβ_{11-25} peptide fragment. *Structure.* 11:915–926.

77. Bond, J. P., S. P. Deverin, H. Inouye, O. M. A. El-Agnaf, M. M. Teeter, and D. A. Kirschner. 2003. Assemblies of Alzheimer's peptides Aβ_{25-35} and Aβ_{31-35}: reverse-turn conformation and side-chain interactions revealed by x-ray diffraction. *J. Struct. Biol.* 141:156–170.

78. Zanuy, D., B. Ma, and R. Nussinov. 2003. Short peptide amyloid organization: stabilities and conformations of the islet amyloid peptide NFGAIL. *Biophys. J.* 84:1884–1894.

79. Miller, S., A. M. Lesk, J. Janin, and C. Chothia. 1987. The accessible surface area and stability of oligomeric proteins. *Nature.* 328:834–836.